

Vibration signal characterization of underpass bridge using time-frequency representation method for condition-based maintenance purpose

W. Caesarendra ^{1,2}, M.D. Surindra ^{1,3}, S.A. Putra ⁴, J. Zaini ¹

¹ Universiti Brunei Darussalam, Faculty of Integrated Technologies,
Jalan Tungku Link, Gadong BE1410, Brunei Darussalam.
e-mail: wahyu.caesarendra@ubd.edu.bn

² Universiti Brunei Darussalam, Institute of Applied Data Analytics,
Jalan Tungku Link, Gadong BE1410, Brunei Darussalam

³ Politeknik Negeri Semarang, Department of Mechanical Engineering,
Jalan Prof. Sudharto, SH, Semarang, 50278, Indonesia

⁴ Telkom University, School of Industrial and System Engineering,
Bandung 40257, Indonesia

Abstract

Bridges are among the important infrastructure to support social and economic activities in the South East Asia region. Monitoring the bridge dynamic is important for regular maintenance. Bridge health monitoring is highly dependent on environmental factors and their utilization, especially the influence of moving loads, such as large vehicles, so they are chosen as crucial parameter factors. There have been widely devoted methods for bridge condition monitoring based on vibration signals using certain signal processing methods. This study aims to investigate the dynamic characteristics of underpass bridges, in particular, the frequency response of the bridge. The initial study is to construct a numerical model of the bridge using the Finite Element Analysis (FEA) method. The frequency response of the numerical model is validated with the time-frequency representation method i.e. Empirical Mode Decomposition (EMD) for underpass bridge vibration data collected from the wireless accelerometer. The result shows the frequency response of the numerical method is detected in the frequency response of the EMD method.

1 Introduction

Bridge construction is a building structure built upon terrain in the form of physical obstacles such as water areas (rivers, straits/sea, and swamps), deep valleys/basins, and surfaces that must be avoided to be crossed, namely roads or railways without blocking the road below. Bridge designs vary in different places, to serve a specific purpose and apply to different situations. Furthermore, variations of bridge design are also influenced by several main factors, namely materials used and funds allocated to build it.

Particular attention was paid to large-scale bridges, which have contributed significantly to socio-economic development. However, it bears the risk of safety problems associated with engineering bridge technology such as cracks and structural damage [1], malfunctions [2], corrosion of materials [3,4], deterioration of performance due to improper design [5], and the influence of other factors affecting uncontrollable such as overloading and collision of trucks [6,7], and natural disasters or erosion of the surrounding soil [8,9]. Bridge damage or disease inevitably affects normal operations and bridge structures face daily emergencies, which might one day collapse.

Visual inspection of the bridge's condition plays an essential role in detecting and evaluating surface defects in the structure over a period of time. Nonetheless, tool-less investigations are slow, laborious, result in quantitative data, and might be unsafe due to their hazardous location. Furthermore, this traditional visual inspection has been highly subjective, relies heavily on the inspector's own ability to make condition assessments, and is insufficient in detecting accurately and in real-time changing of bridge state [10].

The development of an automatic and effective Structural Health Monitoring (SHM) assessment system for bridges, which can continuously report on all weather and environmental conditions, is obligatory for ensuring bridge safety by monitoring short-term and long-term shifts in the bridge construction structure. SHM technology identifies data information by extracting response parameters that describe bridge conditions and applying them to preventive maintenance systems for abnormal analysis, generally based on integrated data and combined sensing networks to detect certain responses at desired points such as displacement, acceleration, strain, and stress. Several researchers have tried to dedicate the development of SHM systems to get areas of potential fatigue and damage-prone structures by investigating key factors based on data response [11]. For an instant, several studies have been published regarding optical fiber-based sensors to observe the damage from structural fatigue and their application to SHM technology [12,13]. Analysis of dynamic characteristics against deterioration of material quality on modal curvature of bridges for classification and localization of damage due to environmental changes was also investigated using Principle Component Analysis (PCA). Mode Shape Curvature (MSC) was adopted to add a vibration feature, thereby increasing the quality of the SHM system to a higher level [14]. Meanwhile, Bellinno et al [15] adopted PCA to analyze the frequency variation as an indication of failure, regardless of site conditions, more, PCA was developed by Yang et al [16] with Characteristics Narrow Dimension (CND) which is equipped with damage features to identify damage bridges in various environmental temperatures.

Other studies have compared non-destructive experimental testing with advanced numerical procedures, from beginning construction to running time, whether there is performance degradation of SHM. Therefore, the results of numerical research in the form of bridge health predictions must be truly related to the actual situation, even if a bridge collapses, the causal variables can be predicted and anticipated not to happen. Domenico et al [17] have carried out a case study on the Zappulla multi-span viaduct concrete bridge in the municipality of Rocca di Capri Leone, in southern Italy, from the Tyrrhenian Sea approximately 2 km away. The researchers have implemented parameter measurements in the field and compared them with numerical simulations to control quality and measure deck safety in concrete bridges. Khodair et al [18] have reported experimental investigations and numerical analysis of the Scotch Road integral abutment bridge located in Trenton, NJ, USA. Several spots on the bridge are instrumented by installing a strain gauge, tiltmeter, displacement transducer, temperature sensor, and soil pressure cell. The measurement results are simulated into a non-linear three-dimensional finite element to evaluate the bridge structure against changes in thermal and axial stresses in the piles. Another study was conducted by Valaskova et al [19] who have dedicated research related to the experimental and numerical analysis of the natural frequency of the bridge construction structure. They have taken the research object of the bridge located at the address, state road III/01,170, between two villages, Mojš and Varín, Slovak Republic. The bridge also has a double-track railway linking the city of Žilina-Košice. The research has offered a solution for determining the natural frequency through an equalized and distributed mass mode, on a continuum basis.

Maintenance of bridge infrastructure requires a strategy, and a large budget to ensure its safety operations. Although the government's response is still lacking, in recent years, many researchers have focused on developing SHM from a manual assessment system to an inspection using sensors that operate continuously, and comprehensively, even based on cloud monitoring, as revealed in the reference above. The researchers also validated and predicted bridge conditions through finite element analysis and then included them as part of the SHM.

This research investigates the underpass bridge in Cisomang village as a case study, which is part of the Purbaleunyi highway road, and the daily workload is quite heavy because it is located at the main road point connecting two major cities i.e. Jakarta and Bandung. This research activity also refers to the research of Jin et al [20], in which they have revealed that underpass bridge technology allows several new problems to emerge, such as water resistance and structural safety in longitudinal joints under static load conditions, vehicular traffic in underpass tunnels, and dynamic loads on the road surface in the long term due to the effect of vehicle movement rates. In this research, a sensor set is installed on the bridge to capture the

frequency response data and build it into a numerical model. The influence of passing vehicles is identified and selected only for heavy and loaded vehicles such as trucks because it will cause a significant vibration effect.

2 Theory of Empirical Mode Decomposition (EMD) method

The selected time-frequency representation method for this study is Empirical mode decomposition (EMD) [21], which has been proven to be adaptable in non-stationary and non-linear signal applications (e.g. Braun and Feldman [22]). The main function of EMD is to decompose the original vibration signal into several signals which have specific frequencies called intrinsic mode functions (IMFs) based on the enveloping technique (Hilbert-Huang transform). The results of IMFs are from high frequencies to low frequencies. In condition monitoring of rolling element bearing, EMD is used to reveal the frequency content of the vibration signal by decomposing the original signal into several IMFs. In preliminary studies on condition monitoring [23,24], the original EMD [21] is used for the non-stationary slew bearing data. According to the EMD capabilities to decompose a vibration signal, it will be potentially used to reveal a low-frequency signal in bridge monitoring after reduced high frequencies.

The EMD method is a necessary strategy for simplifying various kinds of data into a set of intrinsic mode functions (IMF) by applying Hilbert spectral analysis. The EMD algorithm has been applied as a vibration signal processing method for bridge damage detection [25,26], to detect stiffness changes during the vehicle-bridge interaction [27], and to identify bridge frequency response in a passing vehicle [28]. The focus of the EMD method is to empirically decompose this intrinsic oscillation mode with its characteristic time domain in the data, and then accordingly decompose signal data. Extreme oscillations with no zero-crossing can be ignored and are known as the shifting process. Therefore the EMD algorithm considers signal wave oscillations in a very localized and focused area, separated from the overlapping data into local time domain components. Signal data $x(t)$ decomposed by the EMD method into Intrinsic Mode Function (IMF), $c_i(t)$ and residual, $r(t)$ thus signal $x(t)$ can be represented as follows:

$$x(t) = \sum_{i=1}^N c_i(t) + r(t) \quad (1)$$

The sifting process of the EMD algorithm consists of several steps which can be stated as follows:

The first step focuses on Intrinsic Mode Function (IMF),

1. Local extreme values such as maximum and minimum points are identified and then these extreme points are connected with a cubic spline to obtain the upper and lower envelopes. Each of the envelopes must include all the extremes of the local data position.
2. The average value of the two envelopes is obtained by calculation as a function of time and is denoted by the mean, $m_1(t)$.
3. The subtraction between the data signal $x(t)$ and the mean value of $m_1(t)$ can be written in the relation as follows

$$h_1(t) = x(t) - m_1(t) \quad (2)$$

where the symbol $h_1(t)$ is taken into account in the main definition of the IMF.

4. The first IMF must be made more accurate by making $h_1(t)$ the new data signal, determining the upper and lower envelope data points, and the new mean value of $m_2(t)$ so that a new equation is obtained, specifically,

$$h_2(t) = h_1(t) - m_2(t) \quad (3)$$

Like the previous process, $h_2(t)$ is defined as a new signal data, and the process is repeated continuously or is known as an iterative process. This iterative process is denoted by k until the termination condition is fulfilled. The symbol $h_k(t)$ represents the first IMF, recognized by $H_1(t)$.

The second step focuses on residue,

- To find the second layer of IMF $H_2(t)$, with the same sequence of procedures as in steps 1 to 4, the decomposition process analyses the first residual IMF as the following equation:

$$d_1(t) = x(t) - H_1(t) \tag{4}$$

The iteration of the sifting process continues until no variation in the residual or small extreme changes.

3 Research methodology

The bridge used as a case study is the Cisomang Underpass Bridge, in Indonesia as presented in Figure 1. The Cisomang underpass bridge is a bridge located between 6°41'58.6" south latitude and 107°26'01.9" east longitude, which is located in Cisomang Village, Darangdan District, Purwakarta Regency, West Java Province, Indonesia, on the border between Kabupaten Cisomang Purwakarta and West Bandung Regency. This bridge is part of the Purwakarta-Bandung-Padaleunyi (Purbaleunyi) highway road with a length of almost 123 km. It is a panoramic highway road that crosses various hills and ravines, thus requiring a connecting bridge. In addition, the highway road also passes through several residents' roads, so in order not to disturb it, an underpass bridge was built, one of which is in Cisomang.



Figure 1: (a) Red pinpoint shows the location of the Cisomang Underpass-Bridge in Indonesia, on Google maps, (b) Front view of underpass-bridge

3.1 Wireless sensor and vibration data acquisition for measurement

Sun Small Programmable Object Technology (Sun SPOT) is a wireless sensor network with sensor nodes assembled by Sun Microsystems. The hardware uses an ARM architecture 32-bit CPU processor board with an ARM920T core running at 180 MHz as seen in Figure 2. Random-access memory has 512 KB of RAM and 4 MB of flash memory. Further, the IEEE 802.15.4 2.4 GHz Radio has an integrated antenna and a USB interface is included. The sensor equipment consists of a three-axis accelerometer (with 2G and 6G range settings), a temperature sensor, a light sensor, 8 tri-color LEDs, analog and digital inputs, two momentary switches, and 4 high currents output pins. The device adopts a rechargeable 750 mAh 3.7V lithium-ion battery, features 30 uA deep sleep, and battery management is available by software.

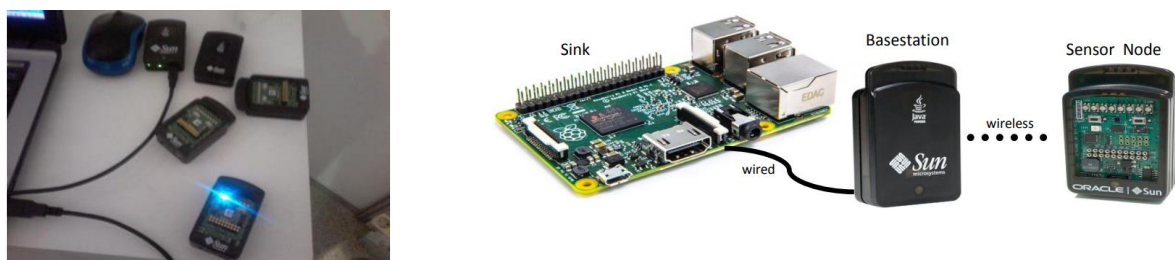


Figure 2: Hardware and sensor node Sun SPOT

Sun SPOT uses the compact Java ME Squawk software which is compatible with the processor even without the operating system. Both Sun SPOT and Squawk VM code are open source and freely accessible. Application management and deployment are handled by the ant script, which can be downloaded from the development environment, and the command line. The device unit uses the IEEE 802.15.4 standard for its sensor network and applies the Java Squawk mode feature.

The real challenge in the data collection process is the flood of data because there is a lot of incoming data. Before the pandemic, in 2019, the Purbaleunyi highway road served 166,574 units of various types of vehicles in one day [29]. This number has not yet been categorized as a type of vehicle, even though the data required is a truck-type vehicle and preferably a loaded truck type. The sensor response must be able to ignore family and personal vehicles or other light vehicles because it will not have a serious vibration effect on the bridge, while trucks with a maximum carrying loads and trucks with loads exceeding the limit will be recorded vibration data as a bridge response. From the side of the sensing device, the sensor node will respond to all the initial data, then it will be sent to the sink node and generate big data for processing in the Wireless Sensor Network (WSN) and server operations, as illustrated in Figure 3. The data sent to the sink node will be disaggregated, not always reflecting the occurrence of important events [29].



Figure 3: (a) Installation of the accelerometer sensor on the side of the bridge (b). Sensor-detected vibration response display

3.2 Vibration data retrieval research procedures

The sensing protocol in the network based on the multi-agent system in the WSN which is applied to the Cisomang Underpass Bridge has used a sleep, standby, and active mode strategy to save system power consumption. The test equipment is designed as an integrated work between an accelerometer sensor (ACC) wireless node and a weight-in-motion (WIM) node based on a load sensor with a sensor placement scheme on two individual bridge spans [30], as presented in Figure 4.

The power supply is connected to the solar cell as backup power and supplies electrical energy to the WIM, while the ACC sensor nodes are distributed in the desired place to get the vibration response of the bridge. A minicomputer, which is a sink node in the form of an electronic circuit board, is tasked with receiving, processing, and storing vibration response data detected by the ACC sensor node. Next, the Sink node will integrate communication with the cloud server.

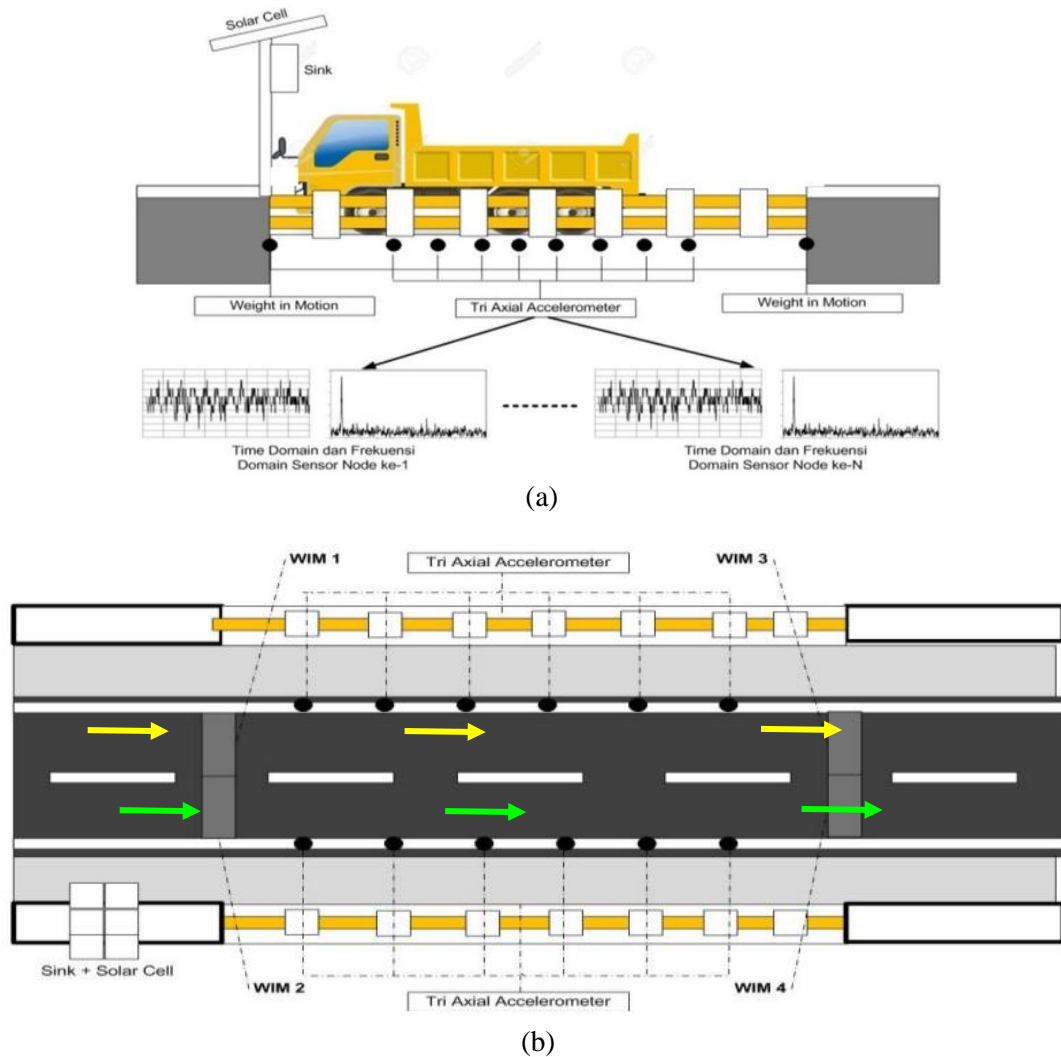







Figure 4: (a) Peak, amplitude identification, and placement of the bridge sensing system. (b) As seen above, the application of WIM, ACC, and sinks including solar cells as backup power

The development of the work system is divided into WIM nodes as data sorters for vehicle types, while the ACC sensor node reads the frequency response of the Cisomang underpass bridge. The types of trucks that pass through the bridge are classified using a neural network by the WIM agent in the classification section into 5 categories, namely type I, II, III, IV, and V such as the highway entry tariff group. Meanwhile, the types of vehicles in group 1 are only buses because the types of small vehicles such as private and family cars are ignored, as presented in Table 1 referenced by the WIM classifier and then processed further online in the data center.

Table 1: Types of motor vehicles on highway roads [31]

Category	Transportation type	Truck Identification
Type I	Bus	
Type II	Truck with 2 (two) axles	
Type III	Truck with 3 (three) axles	
Type IV	Truck with 4 (four) axles	
Type V	Truck with 5 (five) axles	

3.3 Finite element model of the Cisomang underpass bridge

The Cisomang underpass bridge was modeled on the finite element with the CSiBridge 2017 bridge software platform to investigate the behavior of girder boxes and slab concrete bridges, as depicted in Figure 5. CSiBridge software is a tool program to integrate computers with modeling, analyzing, and designing bridge structures. Some researchers use it in their research to investigate cases such as Gupta et al [32] and Mohseni et al [33].

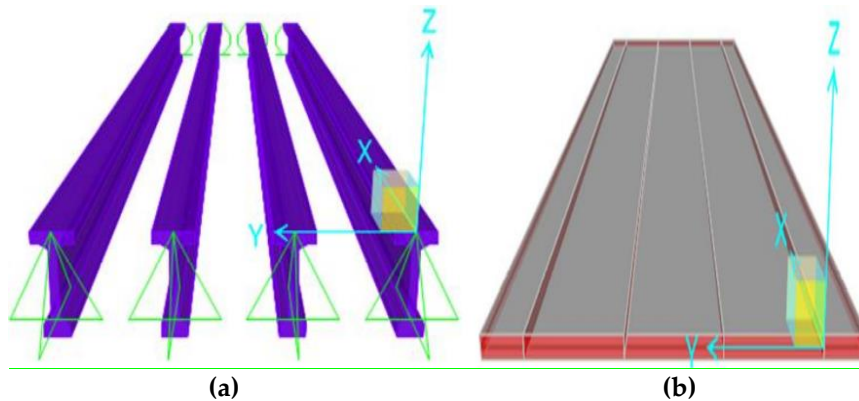


Figure 5: FEA model of Cisomang Underpass Bridge (front view): (a) Girder frame elements; (b) Girder concrete slab

The minimum compressive strength of bridge concrete is 41.5 MPa for box girders and 30 MPa for slab concrete. Above the girder box, there is a concrete slab as a floor with a length of 30 m and 12.6 m respectively with a thickness of 0.36 m. The components of this underpass bridge are pre-stressed girding where the fabrication is done offsite, while the properties of the concrete are presented in Table 2.

Table 2: Material properties of Underpass Bridge at Cisomang

Element	Material	Property			
		Density (kg.m ⁻³)	Elasticity (Mpa)	Quality (MPa)	Poisson Ratio
Girder beam	Concrete	2,400	30,277	41.5	0.2
Concrete plate	Concrete	2,400	25,741	30	0.2
Tendon	Steel	7,850	200,000	1,860	-

4 Result and discussion

During the experiment by installing the ACC sensor on the Cisomang underpass bridge, a lot of bridge response data has been entered, although, various obstacles have also been encountered such as scorching heat from the sun, rainwater, and problems with electricity. The collected bridge vibration response data were analyzed by decoding the raw data using the EMD technique and validated by simulating using FEM, as described below:

4.1 FEA of the underpass bridge Cisomang

FE approach by building a prototype bridge model as in Figure 6, and simulating its operation. If there is a design change, it is easy to change the numerical parameters and maximize the simulation to a state close to the real one.

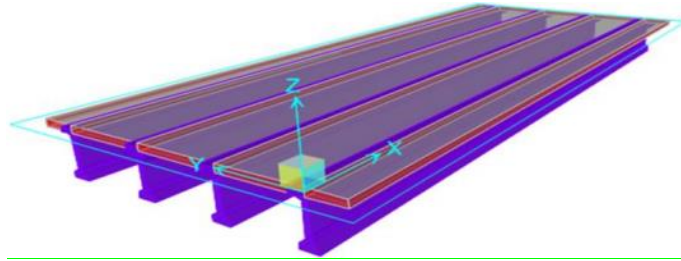


Figure 6: 3D view FEA model of Cisomang Underpass Bridge (3D view).

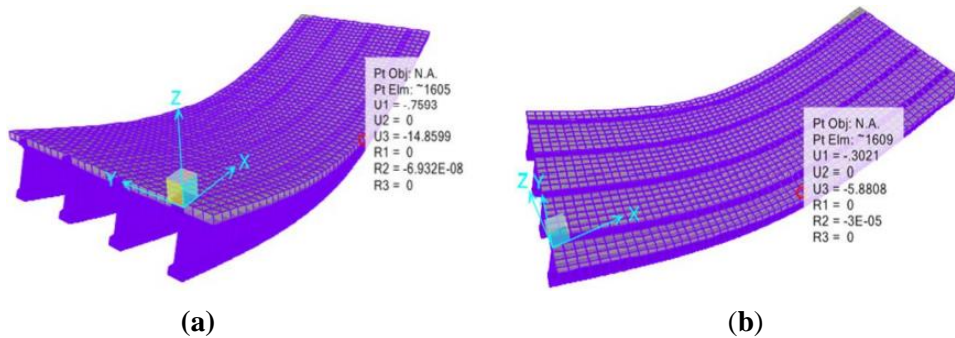


Figure 7: FEA analysis: (a) Bridge deflection due to its weight; (b) Bridge deflection under pre-stressed load.

Testing of the underpass bridge model is carried out by providing static and dynamic loads. The static load applied to the bridge is the weight of the bridge itself which consists of the weight of the concrete slab, girder box, and pre-stressing load, as presented in Figure 7. From the statistical analysis of the simulation results, it has been proven that the load can be accommodated with a maximum deflection of 14.85 mm in the middle of the bridge. While the ability of the bridge increases better with a deflection of 5.88 mm if the pre-stressing force is added to the operational system.

In terms of dynamic analysis, in Figure 8, the response of the Cisomang underpass bridge model is measured when trucks cross it. The frequency generated in the FE analysis is 4.732 Hz and becomes the reference frequency to determine normal bridge conditions.

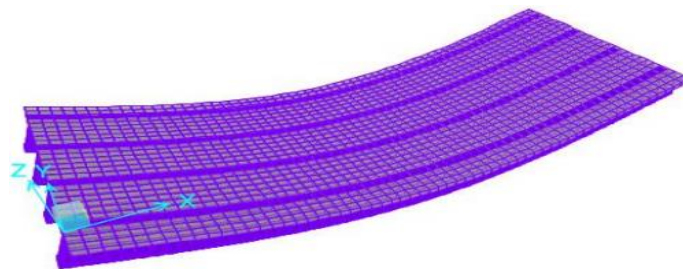


Figure 8: The mode shape of the first fundamental frequency of the bridge.

4.2 Empirical mode decomposition (EMD) results

The raw vibration signal of the Cisomang Underpass Bridge is processed using the EMD method by implementing data point tracking of the signal waveform, especially on the upper and lower envelope sides of the signal to generate IMF components. The decomposed vibration signals of the IMFs were transformed into the frequency domain using FFT. Meanwhile, classification of vehicle types is also carried out, as a result of detecting vehicle types and frequency responses could be captured by the SHM system.

4.2.1 Bus vehicle over the bridge

When the bus crosses the bridge in the left lane, WIM 1 sensor detects the presence of the vehicle and activates the accelerometer node while confirming a vehicle type with WIM 2. Vibration signals are decomposed into 4 IMFs and presented in Figure 9.

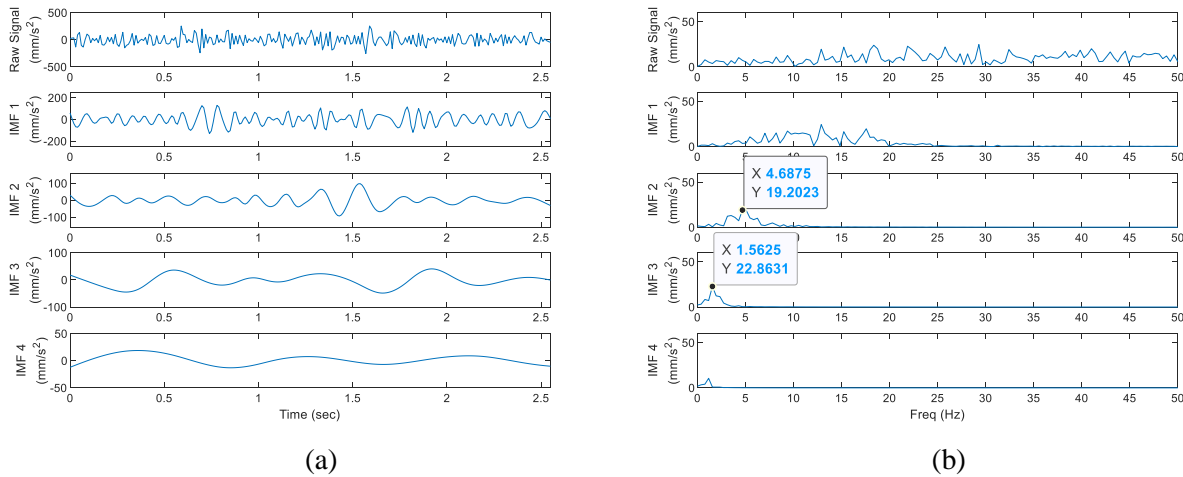


Figure 9: EMD decomposition results in vibrations when the bus over the bridge in (a) time and (b) frequency domain

The acceleration response in the time domain of the vehicle truck shown in Figure 9 in the 'raw signal' box located at the top, will be decomposed using EMD to produce the IMF 1 and 2 components, and the final residue, IMFs 3 and 4, as shown in the figure below the raw signal. It could be roughly observed that the data are separated according to the vibration content which appears to oscillate evenly throughout the observations and does not provide significant fluctuation information of the vibration response in the time and frequency domain, as seen in IMF 1.

Overall, the behavior of the IMF signal can be observed that the data is divided based on the content of the frequency from high to low sequentially. The IMF 1 oscillation component has not seen serious fluctuations, only an increase from the 5 Hz frequency, followed by a peak at about an acceleration of 20 mm/s² and tends to vibrate steadily up and down until the frequency is close to 20 Hz. The second IMF decomposition result has brought a more useful vibration message, which in the observed dominant frequency at 4.688 Hz (~4.7 Hz) as indicated as a black point with a square indicator, shows an amplitude of about 19.202 mm/s². As for further analysis, the third IMF has scored a frequency of 1.562 Hz at a wavelength of 22.863 mm/s², higher than the second IMF.

4.2.2 Two axles truck over the bridge

The first four IMFs for bridge vibration response signals when a two-axle truck crosses the bridge were obtained using EMD and the results are presented in Figure 10. When composing the raw signal, the first IMF was obtained which consisted of a core vibration signal with noise, so it was still unable to read signals in the time and frequency domains easily, even though signal decoding had occurred and managed to remove the interfering signal well. Analysis of the 2nd IMF image has shown the prominent FFT spectrum and is quite easy to see. The position of the detected frequency point is 4.688 Hz with a wave acceleration of 33.074 mm/s². The vibration spectrum is close to the normal vibration recorded in the FEA simulation of 4.732 Hz.

Meanwhile, the decomposition signal at IMF 3 shows a lower frequency than IMF 2 with also lower amplitude. The IMF 3 shows the frequency is 1.953 Hz with a vibration amplitude of 18.969 mm/s². The

frequency value is far from the detected fundamental frequency from FEM analysis as indicated in IMF 2 at 4.688 Hz.

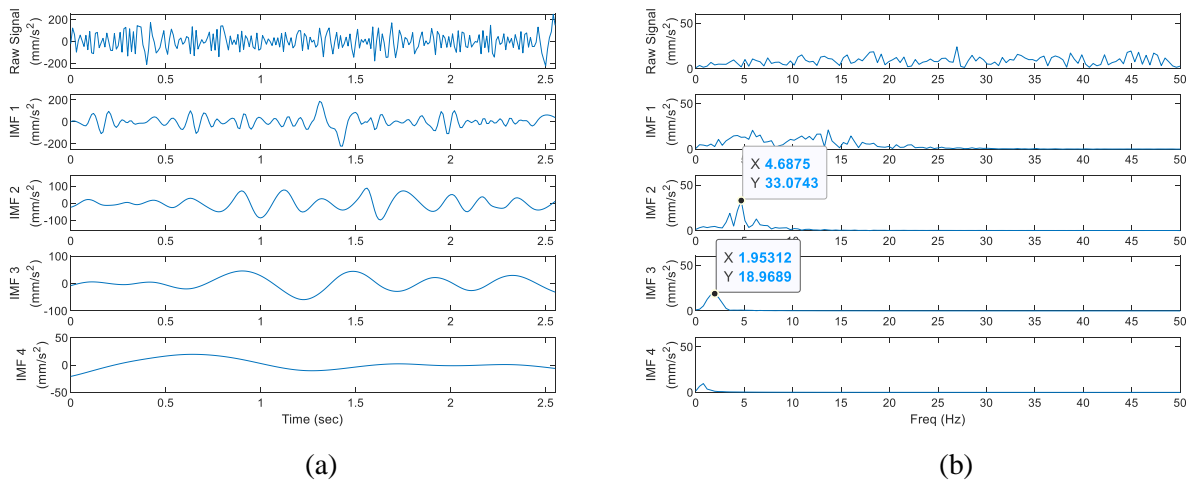


Figure 10: EMD decomposition results in vibrations when two axles truck over the bridge in (a) time and (b) frequency domain

4.2.3 Three axles truck over the bridge

The three-axle truck passes over the bridge and provides vibrational excitation. The vibration response is described in the four IMFs in the domain of time and frequency as provided in Figure 11. The three-axle truck has experienced quite different conditions from before, where the results of the first IMF have detected a significant frequency harmonic reaching 7.42 Hz with a wave oscillation of 21,6876 mm/s² and becomes the highest frequency at a big enough swing amplitude spectrum signal. This point has provided crucial information, although from the beginning of the composition noise appeared disturbing to around the frequency of 20 or 30 Hz. The second IMF has described a signal condition that has decreased by 4.688 Hz with an oscillation amplitude of 64,736 mm/s², followed by the composition of the third IMF which has recorded a frequency of 2.734 Hz at an amplitude of 15,925 mm/s², which has been reduced and neglected. Therefore, the furthest deviation from the equilibrium point in the sinusoidal waveform has occurred in the decoding of the second IMF signal, a record of gigantic amplitude swings.

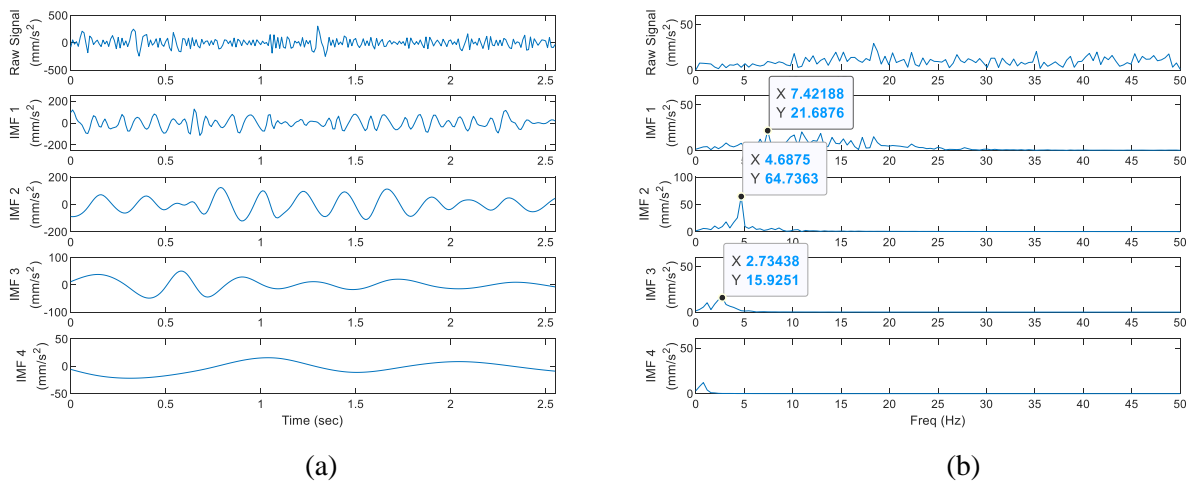


Figure 11: EMD decomposition results in vibrations when three axles truck over the bridge in (a) time and (b) frequency domain

The vibration duration has also shortened between the start of the compositing process until the frequency approaches 10 Hz, as presented in the second layer IMF. Subsequent frequency lengths, in the third and fourth layer IMF breakdown, have been illustrated progressively shorter with records at 4 Hz and 2 Hz, respectively. Furthermore, for the third and fourth IMF, the spectrum of the FFT signal has recorded an extremely low frequency, accordingly, it has been ignored and considered residual.

4.2.4 Four axles truck over the bridge

The vibration excitation provided by the four-axle truck has resulted in the response signals which are arranged into four IMF graphs in the time and frequency domains as presented in Figure 12. When the four-axle truck crosses the bridge, the signal decomposes in the second stage of the IMF register start at the beginning graph and growing to a peak at 4.68 Hz vibration with an accelerating wave at 76.2 mm/s², then ending at about 10 Hz, as shown in Figure 12. On the other hand, the IMF 1 decomposition has given unclear information about the time and frequency domain of the signal because it starts from the beginning of the noise decomposition which has developed even though the signal waveform has been reduced due to the decoding of the signal from the intruder. In addition, the frequency spectrum signal has been caught by the frequency monitoring system at 3.125 Hz with an amplitude swing of 79.777 mm/s². Response readings with moderately high scores have attracted attention for further investigation.

When Signal processing continued for IMF 3 has produced a frequency of 1.953 Hz at a wave acceleration of 28.511 mm/s², almost 50 percent of the IMF 2 frequency decomposition result. Furthermore, the decomposition process at IMF 4 level has generated around the frequency of 1 Hz at a wave acceleration of about 14 mm/s², getting smaller and the IMF time-domain almost a straight line. Thus IMF 3 and 4 can be ignored and pinned as residuals.

Another noticeable information obtained from the EMD result is the high amplitude at a low frequency that appeared in IMF 2. This feature has not been presented in IMF 2 results of bus, 2-axles truck, and 3-axles truck. This indicated that the increasing weight of the vehicle that passes through the bridge effect the dominant amplitude of the IMF 2.

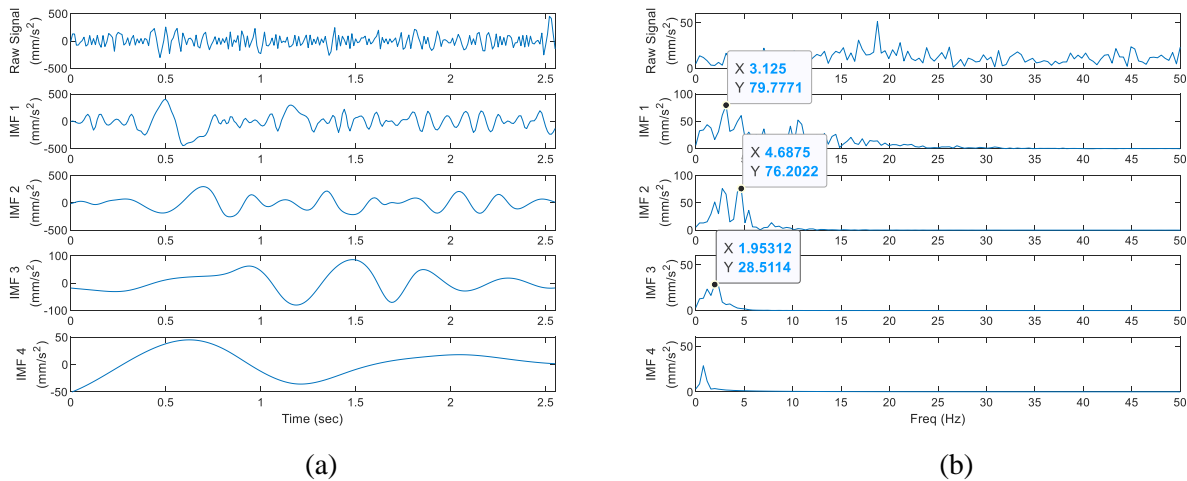


Figure 12: EMD decomposition results in vibrations when four axles truck over the bridge in (a) time and (b) frequency domain.

4.2.5 Five axles truck over the bridge

The result of compiling the vibration response signal into four IMF graphs in the time and frequency domains as presented in Figure 13, is the vibrational excitation of a five-axle truck passing through the bridge. The raw signal has been decomposed in IMF 1 with imperfect results due to interfering signals and noise on the graph of the time and frequency domain along with the start of decomposition to about 20 Hz.

However, the FFT signal spectrum has stored a fairly large amplitude wave of 61.8756 mm/s^2 at a frequency of 4.6875 Hz , the position of the point must receive special attention.

The decomposition continues in the second step and produces IMF 2 where the graph has provided useful information for monitoring the condition of the bridge. The vibration signal begins to develop at a frequency of 2 Hz and reaches its peak at a frequency of 4.6875 Hz with a wave acceleration of 91 mm/s^2 , then the signal decreases until it disappears at a frequency of about 10 Hz . The peak position in the 2nd IMF decomposition has been documented by an increase in wave amplitude as high as 30 mm/s^2 , the swing of the Cisomang underpass bridge which develops rapidly when a 5-axle truck passes through it.

The decomposition of IMF 3 has resulted in a lower frequency than IMF 2, of 1.56 Hz at an acceleration wave of 20.38 mm/s^2 . This decomposed vibration response continues to decrease in IMF 4 so that both IMFs can be ignored and considered residual.

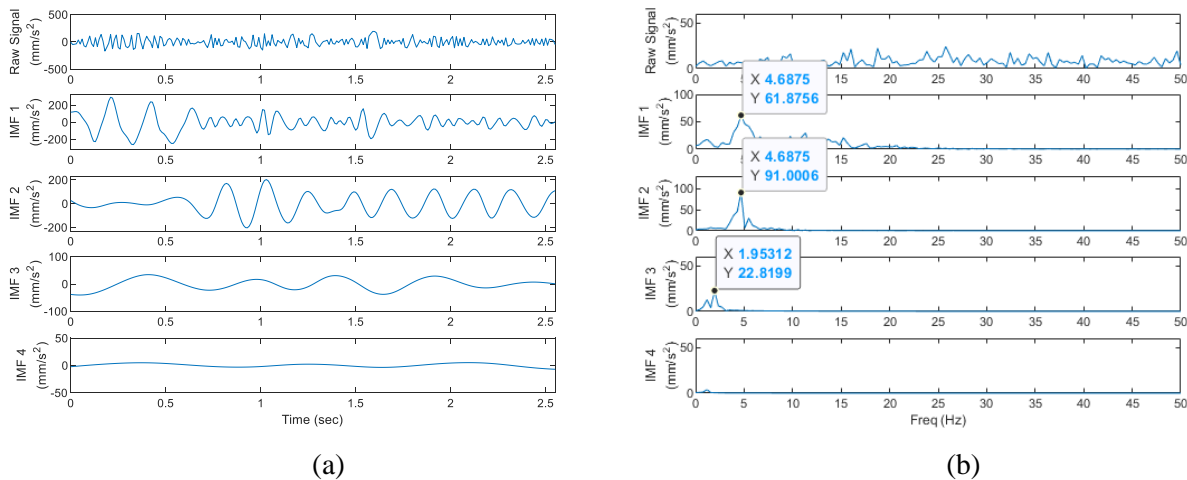


Figure 13: EMD decomposition results in vibrations when five axles truck over the bridge in (a) time and (b) frequency domain.

4.2.6 Comparison of the frequency and amplitude of various types of vehicles

The signal processing method with EMD has provided a comprehensive picture of the response behavior of the Cisomang underpass bridge when various vehicles pass through it. The vibration signal characterization of the 5 vehicle types is presented in Figure 14, which shows the fundamental frequency of the vibration signal i.e. $\sim 4.7 \text{ Hz}$, and the amplitude swing of the particular fundamental frequency on the bridge.

Bridge resonance has been dynamically fluctuating, as well as the distance of the turbulent amplitude wave when various vehicles pass through the bridge. Analysis comparative of vibration signal decomposition in Figure 14 involves frequency and amplitude on the bridge due to an excitation bus and truck in various axles. Bridge resonance with a fundamental frequency of 4.678 Hz has occurred when all types of vehicles pass through the bridge, furthermore, this frequency is closest to the simulation in FEA. Overall, at the same frequency, displacement of wave amplitude increases starting with the bus at $19,202 \text{ mm/s}^2$, followed by a two-axle truck, and almost doubles when the three-axle truck crosses the bridge from $33,074 \text{ mm/s}^2$ to $64,73 \text{ mm/s}^2$. The four-axle truck causes swinging vibration amplitude to raise at 76.202 mm/s^2 and reaches a peak at 91.006 mm/s^2 when the five-wheel axle truck crosses the bridge.

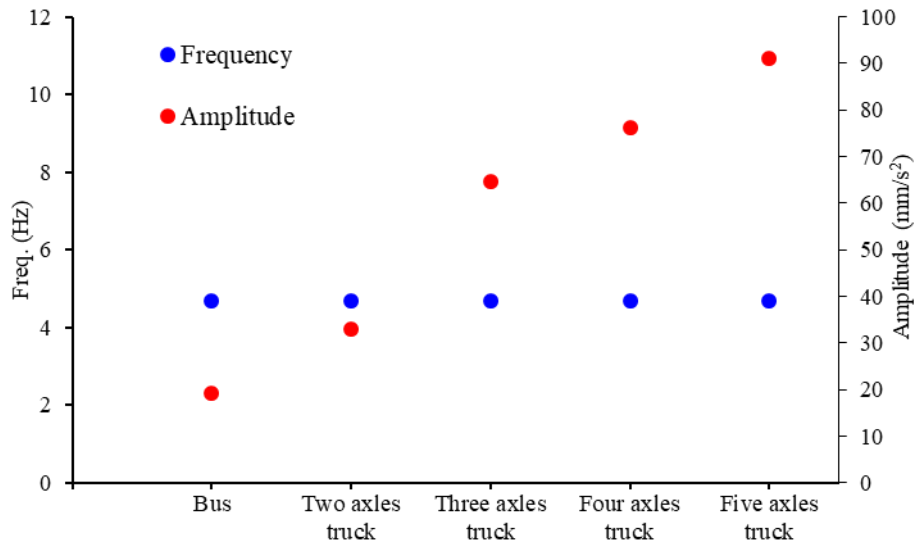


Figure 14: Vibratory response of the bridge from the excitation of various vehicle types

5 Conclusion

In this study, the dynamic behavior of the Cisorang underpass bridge was observed by installing sensor equipment to implement the monitoring method as part of the SHM system. The bridge consisting of concrete slabs and girder boxes has become the scenario for trucks crossing the bridge and providing excitations that are captured by weight and vibration sensors.

Simulations using FEA have been carried out by determining the condition of the truck with heavy loads, while the frequency result is 4.732 Hz as a benchmark and the normal frequency for the operation of the Cisorang underpass bridge. Moreover, Empirical mode decomposition (EMD) has been employed as a signal separator to get the actual signal generated by vehicles passing through the bridge.

Trucks of various types have recorded an FFT signal spectrum of around 4.68 Hz, which is close to the normal frequency generated from the FEA simulation of 4.732 Hz. Meanwhile, the amplitude of the vehicle excitation has given the results of signal decomposition which rises an increasing vehicle's weight.

Meanwhile, the bridge amplitude escalates linearly with the increase in the truck wheel axle, because it is related to the rise total gross weight of the vehicle. To conclude, at the same bridge frequency, the increase in the gross weight of the vehicle results in a growing magnitude of swing amplitude wave.

Acknowledgments

This research was funded by UNIVERSITI BRUNEI DARUSSALAM, grant number UBD/RSCH/1.11/FICBF(b)/2020/003

References

- [1] M. Domaneschi, C. Pellecchia, E.D. Iuliis, G.P. Gimellaro, M. Morgese, and A.A. Khalil, "Collapse analysis of the Polcevera viaduct by the applied element method," *Engineering Structures*, vol. 214, pp. 110659, 2020.
- [2] J. Sun, J. Zhang, W. Huang, L. Zhu, Y. Liu, and J. Yang, "Investigation and finite element simulation analysis on collapse accident of Heyuan Dongjiang Bridge," *Engineering Failure Analysis*, vol. 115, pp. 104655, 2020.

- [3] X. Han, D.Y. Yang, and D.M. Frangopol, "Optimum maintenance of deteriorated steel bridges using corrosion resistant steel based on system reliability and life-cycle cost," *Engineering Structures*, vol. 243, pp. 112633, 2021.
- [4] L. Deng, W. Yan, and L. Nie, "A simple corrosion fatigue design method for bridges considering the coupled corrosion-overloading effect," *Engineering Structures*, vol. 178, pp. 309-317, 2019.
- [5] L. Anania, A. Badalà, and G. D'Agata, "Damage and collapse mode of existing post tensioned precast concrete bridge: The case of Petrulla viaduct," *Engineering Structures*, vol. 162, pp. 226-244, 2018.
- [6] R.W. Li, D.S. Cao, H. Wu, and D.F. Wang, "Collapse analysis and damage evaluation of typical simply supported double-pier RC bridge under truck collision," *Structures*, vol. 33, pp. 3222-3238, 2021.
- [7] R. Cao, A.K. Agrawal, and S. El-Tawil, "Overheight impact on bridge: A computational case study of the Skagit River bridge collapse," *Engineering Structures*, vol. 237, pp. 112215, 2021.
- [8] L. Sakellariadis, I. Anastasopoulos, and G. Gazetas, "Fukae bridge collapse (Kobe 1995): revisited: New insights," *Soil and Foundations*, vol. 60, pp. 1450-1467, 2020.
- [9] Q. Han, X. Du, J. Liu, Z. Li, L. Li, and J. Zhao, "Seismic damage of highway bridges during the 2008 Wenchuan earthquake," *Earthquake Engineering and Engineering Vibration*, vol. 8, pp. 263-273, 2009.
- [10] V. Gattulli, and L. Chiaramonte, "Condition assessment by visual inspection for a bridge management system," *Computer-Aided Civil and Infrastructure Engineering*, vol. 20, pp. 95-107, 2005.
- [11] A. Rageh, S.E. Azam, and D.G. Linzell, "Steel railway bridge fatigue damage detection using numerical model and machine learning: Mitigating influence of modeling uncertainty," *International Journal of Fatigue*, vol. 134, pp. 105458, 2020.
- [12] M. Lydon, D. Robinson, S.E. Taylor, G. Amato, E.J.O. Brien, and N. Uddin, "Improved axle detection for bridge weigh-in-motion systems using fiber optic sensors," *Journal of Civil Structural Health Monitoring*, vol. 7, pp. 325-332, 2017.
- [13] Y.E. Harmanci, M.D. Spiridonakos, E.N. Chatzi, and W. Kübler, "An autonomous strain-based structural monitoring framework for life-cycle analysis of a novel structure," *Frontiers in Built Environment*, vol. 2, pp. 13, 2016.
- [14] Y. Shokrani, V.K. Dertimanis, E.N. Chatzi, and M.N. Savoia, "On the use of mode shape curvatures for damage localization under varying environmental conditions," *Structural Control Health Monitoring*, vol. 25, pp. e2132, 2018.
- [15] A. Bellino, A. Fasana, L. Garibaldi, and S. Marchesiello, "PCA-based detection of damage in time-varying systems," *Mechanical Systems and Signal Processing*, vol. 24, pp. 2250-2260, 2010.
- [16] C. Yang, S. Zhang, Y. Liu, and K. Yu, "Damage detection of bridge under changing environmental temperature using the characteristic of the narrow dimension (CND) of damage features," *Measurement*, vol. 189, pp. 110640, 2022.
- [17] D.D. Domenico, D. Messina, and A. Recupero, "Quality control and safety assessment of prestressed concrete bridge decks through combined field test and numerical simulation," *Structures*, vol. 39, pp. 1135-1157, 2022.
- [18] Y. Khodair, and S. Hassiotis, "Numerical and experimental analyses of an integral bridge," *International Journal of Advanced Structural Engineering*, vol. 5, pp. 1-12, 2013.
- [19] V. Valaškova, and J. Melcer, "Bridge natural frequencies, numerical solution versus experiment," *Applied Sciences*, vol. 12, pp. 1765, 2022.
- [20] Z. Jin, T. Q. and X. Liang, "Evaluation of the structural and waterproof performance of a precast and assembly underpass under long-term surface dynamic loads," *Tunnelling and Underground Space Technology incorporating Trenchless Technology Research*, vol. 115, pp. 104047, 2021.

- [21] N.E. Huang, Z. Shen, S.R. Long, M.C. Wu, H.H. Shih, Q. Zheng, N.C. Yen, C.C. Tung, and H.H. Liu, "The empirical mode decomposition and the Hilbert spectrum for nonlinear and non-stationary time series analysis," *Proceedings of the Royal Society London A 454*, p. 903-995, 1998.
- [22] S. Braun, and M. Feldman, "Decomposition of non-stationary signals into varying time scales: Some aspects of the EMD and HVD methods," *Mechanical Systems and Signal Processing*, vol. 25, p. 2608-2630, 2011.
- [23] W. Caesarendra, B. Kosasih, A.K. Tieu, and C.A.S. Moodie, "Circular domain features based condition monitoring for low speed slewing bearing," *Mechanical Systems and Signal Processing*, vol. 45, p. 114-138, 2014.
- [24] W. Caesarendra, P.B. Kosasih, A.K. Tieu, C.A.S. Moodie, and B.-K. Choi, "Condition monitoring of naturally damaged slow speed slewing bearing based on ensemble empirical mode decomposition," *Journal of Mechanical Science and Technology*, vol. 27, pp. 1-10, 2013.
- [25] J. Chen, "Application of empirical mode decomposition in structural health monitoring: Some experience," *Advances in Adaptive Data Analysis*, vol. 1, pp. 601-621, 2009.
- [26] E.J. O'Brien, A. Malekjafarian, and A. González, "Application of empirical mode decomposition to drive-by bridge damage detection," *European Journal of Mechanics - A/Solids*, vol. 61, pp. 151-163, 2019.
- [27] H. Aied, A. González, and D. Cantero, "Identification of sudden stiffness changes in the acceleration response of a bridge to moving loads using ensemble empirical mode decomposition," *Mechanical Systems and Signal Processing*, vol. 66-67, pp. 314-338, 2016.
- [28] L. Zhu, and A. Malekjafarian, "On the Use of Ensemble Empirical Mode Decomposition for the Identification of Bridge Frequency from the Responses Measured in a Passing Vehicle," *Infrastructures*, vol. 4, pp. 32, 2019. I. Susiyanti, "Jasa Marga catat rekor layani volume lalu lintas tertinggi di sepanjang sejarah jalan tol di Indonesia," *Press Release PT JASA MARGA (Persero) Tbk*, no. 122/2019, 10 Juni 2019, <https://www.jasamarga.com/public/id/aktivitas/detail.aspx>, (accessed on 13 April 2022)
- [29] S.A. Putra, B.R. Trilaksono, M. Riyansyah, D.S. Laila, A. Harsoyo, and A.I. Kistijantoro, "Intelligent sensing with multiagent-based wireless sensor network for bridge condition monitoring system," *IEEE Internet of Things Journal*, vol. 6, pp. 5397-5410, 2019.
- [30] S.A. Putra, B.R. Trilaksono, M. Riyansyah, and D.S. Laila, "Multiagent architecture for bridge capacity measurement system using wireless sensor network and weight in motion," *IEEE Transactions on Instrumentation and Measurement*, vol. 70, pp. 1-14, 2021.
- [31] Konten Golongan Kendaraan, based on Kepmen PU No 370/KPTS/M/2007, Kementerian Pekerjaan Umum dan Perumahan Rakyat, Badan Pengatur Jalan Tol, <https://bpjt.pu.go.id/konten/golongan-kendaraan>. (accessed on 14 April 2022)
- [32] T. Gupta, and M. Kumar, "Flexural response of skew-curved concrete box-girder bridges," *Engineering Structures*, vol. 163, pp. 358-372, 2018.
- [33] I. Mohseni, Y. Ahn, and J. Kang, "Development of improved frequency expressions for composite horizontally curved bridges with high-performance steel girders," *Arabian Journal for Science and Engineering*, vol. 44, pp. 4151-4160, 2019.